International Journal of Automotive Technology, Vol. 24, No. 4, pp. 1141-1149 (2023)
DOI 10.1007/s12239–023–0093–7

pISSN 1229–9138/ eISSN 1976–3832

CHATTERING REDUCTION OF SLIDING MODE CONTROL VIA NONLINEAR DISTURBANCE OBSERVER FOR ANTI-LOCK BRAKING SYSTEM AND VERIFICATION WITH CARSIM SIMULATION

Minseong Choi[1)], Kyunghwan Choi[2)], Minsu Cho[3)], Minyoung Lee[4)] and Kyung-Soo Kim[3)*]

[1)]Division of Future Vehicle, KAIST, Daejeon 34141, Korea
[2)]School of Mechanical Engineering, GIST, Gwangju 61005, Korea
[3)]Department of Mechanical Engineering, KAIST, Daejeon 34141, Korea
[4)]Department of Smart Industrial Machine Technologies, KIMM, Daejeon 34103, Korea

(Received 2 November 2021; Revised 9 June 2022; Accepted 10 June 2022)

ABSTRACT–The anti-lock braking system (ABS) is a vehicle safety technology that prevents wheels from locking during braking by tracking the optimal reference slip. Due to the structural characteristics of hydraulic circuits, a brake system has a discontinuous pressure control input which is composed of apply and dump modes. Sliding mode control is a robust control technique that uses discontinuous control input and is being studied expensively. However, sliding mode control has a crucial chattering problem caused by high compensation gain, which leads to high wearing of the mechanical parts. This problem can be alleviated by compensating for unknown disturbances with estimated values. A nonlinear disturbance observer can estimate the system's uncertainty without mathematical model information. Therefore, sliding mode control based on a nonlinear disturbance observer is proposed here, and the simulation results with ABS are compared with the original sliding mode control. Simulations are conducted with high- and low- μ road surface scenarios, and three key performance indicators for evaluations are compared. In conclusion, the brake performance was enhanced and the chattering issue of the sliding mode controller was reduced by proposed method.

KEY WORDS : Anti-lock braking system (ABS), Sliding mode control, Nonlinear disturbance observer, Vehicle safety control, Hydraulic circuits

1. INTRODUCTION

Vehicle safety controls, which include the anti-lock braking system (ABS), the traction control system (TCS) and electronic stability control (ESC), are emerging as interest in electric vehicles and autonomous vehicles increases. ABS, which was first developed in 1945 to reduce the stopping distance of the Boeing B-47 airplane, is being applied and studied not only in the aerospace industry but also in the vehicle industry (Wellstead and Pettit, 1997). The wheel locks up during severe braking on a slippery road surface, which causes a long stopping distance and loss of vehicle stability (Georg, 1995; Lojko and Fuchs, 2002). The main objective of ABS is to prevent the locking of wheels during braking to achieve high brake performance while simultaneously maintaining vehicle stability.

1.1. Principles of Anti-lock Braking System

Figure 1 shows the hydraulic circuit for a typical ABS module, which consists of a motor and pump, 2 accumulators, 6 normally open (NO) valves and 6 normally closed (NC) valves. The FR wheel represents the apply mode. Without operating any valve, brake oil fluid with high pressure is directly transmitted to the brake caliper by pushing the pedal. The RR wheel shows the hold mode, which blocks oil inflow from the master cylinder by using a NO valve. The FL and RL wheels represent the dump mode. By operating the NO and NC valves, the brake oil fluid moves toward the accumulator to reduce the brake pressure and prevent the wheel from locking. Typical normalized longitudinal friction-slip curves for various road surfaces are shown in Figure 2. The simplified slip of the wheel is defined as,

$$\lambda = \frac{\omega_w - \omega_v}{\omega_v} \tag{1}$$

where ω_w and ω_v denote the wheel angular velocity and vehicle angular velocity, respectively. Especially wheel angular velocity ω_w is defined as $\omega_w = r_{eff} \cdot \omega$ where r_{eff} and ω denote effective wheel radius and wheel angular velocity (Jazar, 2017). And effective wheel radius r_{eff} can

**Corresponding author*. e-mail: kyungsookim@kaist.ac.kr

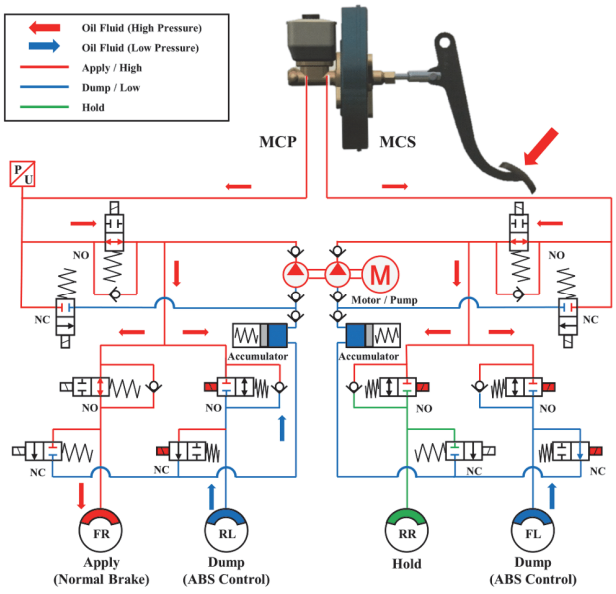

Figure 1. Hydraulic circuit showing overall ABS operation process (Kuang *et al*., 1999; Cai *et al*., 2012).

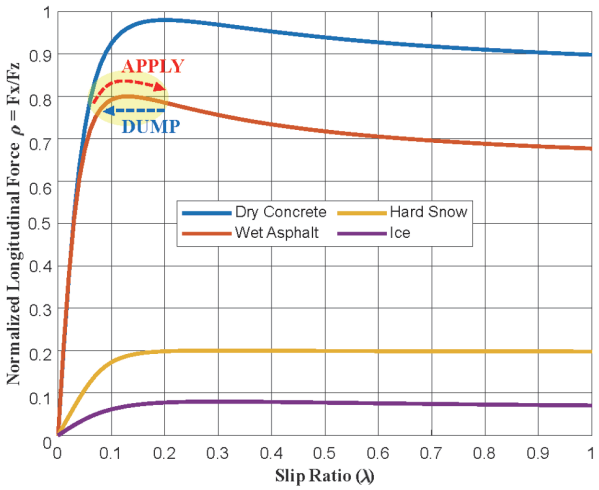

Figure 2. Typical tire longitudinal friction-slip (λ) curve.

be simply written as $r_{eff} = r_o - F_z/k_z$ where r_o, F_z and k_z denote nominal wheel radius, vertical tire load and vertical stiffness of tire. The nominal wheel radius can be obtained from decoding information on the sidewall of tire. But vertical stiffness of tire should be derived from empirical experimental results. The optimal reference slip λ^* for maximum braking performance is given for various road surface types. The key point of ABS is to control wheel slip around the optimal reference slip by repeating the apply, hold and dump modes.

1.2. Research Trends of the Anti-lock Braking System

Rule-based control algorithms are the mainstream in industry since ABS has discontinuous control inputs consisting of apply and dump modes, as previously mentioned (Kienchke and Nielsen, 2000; Bosch *et al*., 1996; Vignati and Sabbioni, 2020). Rule-based control selects thresholds for wheel acceleration ($\dot{\omega}_v$) and wheel slip (λ) and determines apply, hold, and dump motions based on them. However, there are over 600 parameters to tune considering surface types, mu-transitions, and checkerboard and washer board configurations (Choi, 2008). Therefore, many researchers are conducting studies as described below to reduce the tuning variables and increase robustness.

For example, fuzzy logic controls are being studied extensively because of unknown environmental parameters (Will and Zak, 2000; Layne *et al*., 1993). However, employing many fuzzy rules has the disadvantage of making the system more complicated. Therefore, many ways of reducing the fuzzy variables to make the system more simple have been proposed, such as fuzzy sliding mode control (FSMC), adaptive fuzzy control (AFC), the PID-type fuzzy controller, and self-learning fuzzy sliding mode control (SLFSMC) (Lennon and Passino, 1999; Kim and Lee, 1995; Chen and Shih, 2004; Lin and Hsu, 2003). However, issues still exist, such as numerous tuning parameters or long tuning times when applying fuzzy logic control.

Therefore, sliding mode control (SMC)-based algorithms are mainly being studied to save tuning time and ensure robustness (Lin and Hsu, 2003; Unsal and Kachroo, 1999; Kachroo and Tomizuka, 1995). SMC is a representative robust control technique that is not sensitive to parameters or uncertainties of the system. The control input of SMC consists of a term equivalent to canceling the known system dynamics and a term to eliminate uncertainties. The latter is the sign function multiplied by a convergence gain that is larger than the maximum uncertainty of the system. This term may lead to chattering issues near the sliding surface.

1.3. Research Objective of This Paper

In the case of a system with unknown disturbance, severe chattering could occur, which leads to high wear of the mechanical parts. In particular, braking torque is a control input for the anti-lock braking system, so it is directly related to the life of the brake pad. One way to address unknown disturbances is to estimate unknown time-varying disturbances with observers in real time and compensate for them with the estimated values.

A nonlinear disturbance observer (NDOB) can be a solution for estimating time-varying disturbances. It has been reported that uncertainties converge to real values due to system uncertainty. The chattering issue could be reduced by selecting a small convergence gain based on an NDOB. Therefore, sliding mode control based on an NDOB is proposed to address these uncertainties and is validated with

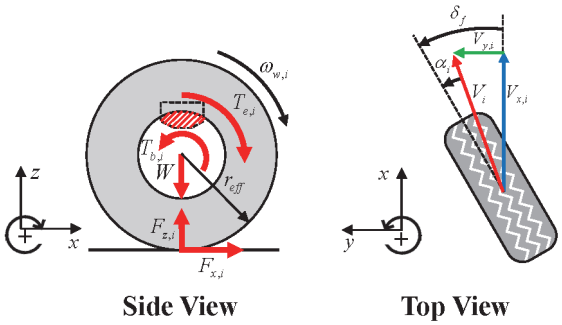

Figure 3. Diagram of the top view and side view of a tire.

simulations in this paper.

This paper is organized as follows: The system dynamics for the anti-lock braking system, nonlinear disturbance observer design and sliding mode controller design are described in Sections 2, 3 and 4, respectively. The simulation environments and results of SMC based on an NDOB are compared with the original SMC for high- and low- μ scenarios in Sections 5 and 6. Finally, a discussion and concluding remarks are given in Section 7.

2. SYSTEM DYNAMICS

In this section, we will describe the dynamic model of an anti-lock braking system. To do this, the tire force model must be defined first. The mathematical models representing the tire force are classified into pure physical, semi-empirical and empirical models (Aripin *et al*., 2014; Yang *et al*., 2013). According to the Pacejka tire model, which is the most widely used for representing empirical models, the longitudinal tire force during braking at the *i-th* wheel is given as follows (Pacejkat and Bakker, 1992).

$$\bar{F}_{x,i} = D_x \sin\left(C_x \tan^{-1}(B_x\Phi_x)\right) + S_{vx} \tag{2}$$

where $B_x = 22 + \frac{F_{z,i} - 1940}{430}$, $C_x = 1.35 - \frac{F_{z,i} - 1940}{16125}$,

$D_x = 1750 + \frac{F_{z,i} - 1940}{0.956}$, $E_x = 0.1$, $S_{hx} = S_{vx} = 0$ and

$$\Phi_x = (1 - E_x)(\lambda_i + S_{hx}) + \frac{E_x}{B_x}\tan^{-1}\left(B_x(\lambda_i + S_{hx})\right)$$

The free body diagram for a driving wheel with a brake system is shown in Figure 3. The wheel dynamics for the rear-wheel drive system can be expressed as follows:

$$\dot{\omega}_{w,1} = \frac{1}{J_{w,1}}(-T_{b,1} - r_{eff}F_{x,1}) + \Delta_1 \tag{3}$$

$$\dot{\omega}_{w,2} = \frac{1}{J_{w,2}}(-T_{b,2} - r_{eff}F_{x,2}) + \Delta_2 \tag{4}$$

$$\dot{\omega}_{w,3} = \frac{1}{J_{w,3}}(+T_{e,3} - T_{b,3} - r_{eff}F_{x,3}) + \Delta_3 \tag{5}$$

$$\dot{\omega}_{w,4} = \frac{1}{J_{w,4}}(+T_{e,4} - T_{b,4} - r_{eff}F_{x,4}) + \Delta_4 \tag{6}$$

where $\omega_{w,i}, J_{w,i}, T_{e,i}, T_{b,i}, \Delta_i$ and r_{eff} denote the angular velocity, momentum of inertia, driving torque, braking torque, modeling error including the rolling resistance and effective rolling radius of the *i-th* wheel, respectively.

Driving torque or braking torque on a pneumatic tire generates a tractive force at the tire-road contact patch (Wong, 2008). This torque produces compression or tension at the tire tread and within the contact patch. As a result, the tire travels less or more distance than it would if it were free rolling, which is called the *slip* phenomenon (Jazar, 2017). The longitudinal slip of the wheel is defined as,

$$\lambda_i = \frac{\omega_{w,i} - \omega_{v,i}}{\omega_{v,i}}, \text{ where } \omega_{v,i} = \frac{V_{t,i}}{r_{eff}}\cos(\alpha_i) \tag{7}$$

$$V_{t,1} = \sqrt{\left(v_x - t_w\dot{\psi}\right)^2 + \left(v_y + l_f\dot{\psi}\right)^2} \tag{8}$$

$$V_{t,2} = \sqrt{\left(v_x + t_w\dot{\psi}\right)^2 + \left(v_y + l_f\dot{\psi}\right)^2} \tag{9}$$

$$V_{t,3} = \sqrt{\left(v_x - t_w\dot{\psi}\right)^2 + \left(v_y - l_r\dot{\psi}\right)^2} \tag{10}$$

$$V_{t,4} = \sqrt{\left(v_x + t_w\dot{\psi}\right)^2 + \left(v_y - l_r\dot{\psi}\right)^2} \tag{11}$$

where v_x, v_y, $\dot{\psi}$, l_f, l_r and t_w denote the longitudinal velocity of the vehicle, lateral velocity of the vehicle, yaw rate of the vehicle, distance from the front axle and rear axle to the center of gravity (CG) and half of the vehicle width track, respectively. α_i and $V_{t,i}$ denote the tire slip angle and tire velocity at the *i-th* wheel. Based on the top-view diagram of the tire shown in Figure 3, the tire slip angles are given as follows:

$$\alpha_i = \delta_i - \xi_i \tag{12}$$

$$\xi_1 = \tan^{-1}\left(\frac{v_y + l_f\dot{\psi}}{v_x - t_w\dot{\psi}}\right) \tag{13}$$

$$\xi_2 = \tan^{-1}\left(\frac{v_y + l_f\dot{\psi}}{v_x + t_w\dot{\psi}}\right) \tag{14}$$

$$\xi_3 = \tan^{-1}\left(\frac{v_y - l_r\dot{\psi}}{v_x - t_w\dot{\psi}}\right) \tag{15}$$

$$\xi_4 = \tan^{-1}\left(\frac{v_y - l_r\dot{\psi}}{v_x + t_w\dot{\psi}}\right) \tag{16}$$

We can differentiate (7) to obtain first-order slip dynamics equations as follows:

$$\dot{\lambda}_i = -\frac{1+\lambda_i}{\omega_{v,i}}\dot{\omega}_{v,i} + \frac{1}{\omega_{v,i}}\dot{\omega}_{w,i} \tag{17}$$

By substituting (3) ~ (6) into (7), we can rewrite the slip dynamics containing $T_{e,i}$ and $T_{b,i}$ as follows:

$$\dot{\lambda}_1 = -\frac{1+\lambda_1}{\omega_{v,1}}\cdot\dot{\omega}_{v,1} - \frac{1}{J_{\omega,1}\omega_{v,1}}\cdot T_{b,1} - \frac{r_{eff}F_{x,1}}{J_{\omega,1}\omega_{v,1}} + d_1 \tag{18}$$

$$\dot{\lambda}_2 = -\frac{1+\lambda_2}{\omega_{v,2}}\cdot\dot{\omega}_{v,2} - \frac{1}{J_{\omega,2}\omega_{v,2}}\cdot T_{b,2} - \frac{r_{eff}F_{x,2}}{J_{\omega,2}\omega_{v,2}} + d_2 \tag{19}$$

$$\begin{aligned}\dot{\lambda}_3 = &-\frac{1+\lambda_3}{\omega_{v,3}}\cdot\dot{\omega}_{v,3} + \frac{1}{J_{\omega,3}\omega_{v,3}}\cdot T_{e,3} - \frac{1}{J_{\omega,3}\omega_{v,3}}\cdot T_{b,3}\\ &-\frac{r_{eff}F_{x,3}}{J_{\omega,3}\omega_{v,3}} + d_3\end{aligned} \tag{20}$$

$$\begin{aligned}\dot{\lambda}_4 = &-\frac{1+\lambda_4}{\omega_{v,4}}\cdot\dot{\omega}_{v,4} + \frac{1}{J_{\omega,4}\omega_{v,4}}\cdot T_{e,4} - \frac{1}{J_{\omega,4}\omega_{v,4}}\cdot T_{b,4}\\ &-\frac{r_{eff}F_{x,4}}{J_{\omega,4}\omega_{v,4}} + d_4\end{aligned} \tag{21}$$

where d_i includes the rolling resistance $(\Delta_i/\omega_{v,i})$ tire modelling error and disturbances. These uncertainties can be estimated by designing a nonlinear disturbance observer, which is introduced in the next section.

3. NONLINEAR DISTURBANCE OBSERVER DESIGN

(18) ~ (21) can be rewritten in nonlinear state space equation form as,

$$\begin{aligned}\dot{\mathbf{x}} &= \mathbf{f(x,u)} + \mathbf{d}\\ \mathbf{y} &= \mathbf{g(x)}\end{aligned} \tag{22}$$

with state vector matrix $\boldsymbol{x} \equiv [\lambda_1 \quad \lambda_2 \quad \lambda_3 \quad \lambda_4]^T$, control input matrix $\boldsymbol{u} \equiv [T_{B,1} \quad T_{B,2} \quad T_{B,3} \quad T_{B,4}]^T$, and unknown time-varying disturbances $\mathbf{d}$, respectively. Disturbances and uncertainties affect the performance and even stability of control systems (Gao, 2014; Li *et al*., 2014). In other words, it is a key objective in control system design to reject disturbances. An NDOB was proposed in (Chen *et al*., 2000) to estimate the unknown time-varying disturbance of system (22),

$$\begin{aligned}\hat{\mathbf{d}} &= \mathbf{z} + \mathbf{L}\mathbf{g}^{-1}\mathbf{(y)}\\ \dot{\mathbf{z}} &= -\mathbf{L}(\mathbf{z} + \mathbf{L}\mathbf{g}^{-1}\mathbf{(y)} + \mathbf{f(x,u)})\end{aligned} \tag{23}$$

where $\mathbf{z} \in R^4$ is the internal state of the nonlinear observer, $\hat{\mathbf{d}} \in R^4$ is the estimated disturbance and $\mathbf{L} \in R^{4\times4}$ is the observer gain to be designed. From the above dynamics, we have

$$\begin{aligned}\dot{\hat{\mathbf{d}}} &= \dot{\mathbf{z}} + \mathbf{L}\mathbf{g}^{-1}\mathbf{(y)}\\ &= -\mathbf{L}(\mathbf{z} + \mathbf{L}\mathbf{g}^{-1}\mathbf{(y)} + \mathbf{f(x,u)} - \mathbf{L}\mathbf{g}^{-1}\mathbf{(\dot{y})})\\ &= \mathbf{L(d - \hat{d})}\end{aligned} \tag{24}$$

Since the NDOB gives the dynamics below, rearranged from (24), the estimated disturbances asymptotically converge to the real disturbances.

$$\frac{\hat{\mathbf{d}}}{\mathbf{d}} = \frac{\mathbf{L}}{sI_{4x4} + \mathbf{L}} \tag{25}$$

There are many techniques to choose observer gain $\mathbf{L}$ that have been proposed in other papers (Chen *et al*., 2000; Sariyildiz and Ohnishi, 2014; Zhu *et al*., 2005). The observation gain should be designed correctly for each system.

The control input can be designed to compensate for uncertainties based on estimated disturbances as follows:

$$\mathbf{T_{B,DOB}} = \mathbf{B}\cdot\hat{\mathbf{d}} \tag{26}$$

where $\mathbf{B}$ is a diagonal matrix $\mathrm{diag}(b_1, b_2, b_3, b_4)$ with elements $b_i = J_{w,i}\cdot\omega_{w,i}$. After compensating for uncertainties, designing a sliding mode controller is described in the next section.

4. SLIDING MODE CONTROLLER DESIGN

Sliding mode controllers are known to be robust to nonlinear systems with uncertainties (Slotine and Li, 1991). For tracking the optimal reference slip set $\boldsymbol{\lambda}^*$, we define the sliding surface and Lyapunov function for each wheel as follows:

$$s_i = (\lambda_i - \lambda_i^*),\ V_i = \frac{1}{2}s_i^2 \tag{27}$$

By differentiating the Lyapunov function, we obtain

$$\dot{V}_i = s_i\cdot\dot{s}_i < 0 \tag{28}$$

For a stable system, the derivative of the Lyapunov function should be negative. Let the differential of the sliding

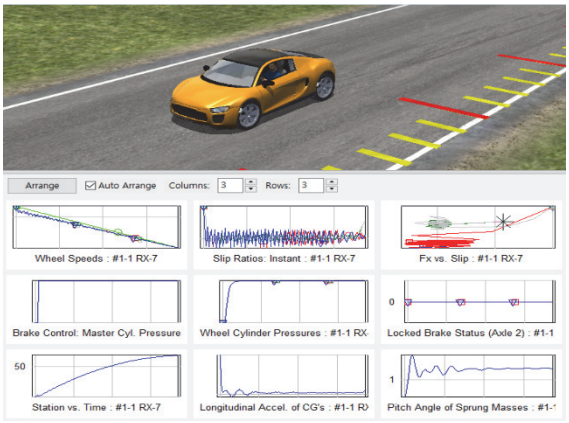

Figure 4. ABS Simulation on CarSim.

Table 1. Test scenarios for high- and low- μ road types. (Pretagostini *et al*., 2020).

Road type	Initial velocity (km/h)	Exit velocity (km/h)	Avg friction coeff.
High friction	130	5	1
Low friction	40	1	0.3

Table 2. Nominal parameters for ABS simulations.

Vehicle mass (m)	1100 kg
Wheel inertia (J_ω)	0.6 $kg \cdot m^2$
Effective radius (r_{eff})	0.353 m
Distance from front axle to CG (l_f)	1.165 m
Distance from rear axle to CG (l_r)	1.165 m
Half width of track (t_w)	0.740 m

surface be as follows, with positive convergence gain K_i:

$$\dot{s}_i = \dot{\lambda}_i - \dot{\lambda}_i^* = -K_i \cdot \mathrm{sgn}(s_i) \tag{29}$$

such that

$$\dot{V}_i = s_i \cdot \dot{s}_i = -K_i \cdot |s_i| < 0 \tag{30}$$

By substituting (18) ~ (21) into (29), the braking torque control input $\mathbf{T_{B,C}} \equiv \left[T_{bc,1} \quad T_{bc,2} \quad T_{bc,3} \quad T_{bc,4}\right]^T$ for tracking λ^* is rewritten as

$$\begin{aligned} T_{bc,1} = & -J_{w,1} \cdot (1+\lambda_1) \cdot \dot{\omega}_{v,1} - r_{eff} \cdot \bar{F}_{x,1} \\ & - J_{w,1} \cdot \omega_{v,1} \cdot \dot{\lambda}_1^* + K_1 \cdot J_{w,1} \cdot \omega_{v,1} \cdot \mathrm{sgn}(s_1) \end{aligned} \tag{31}$$

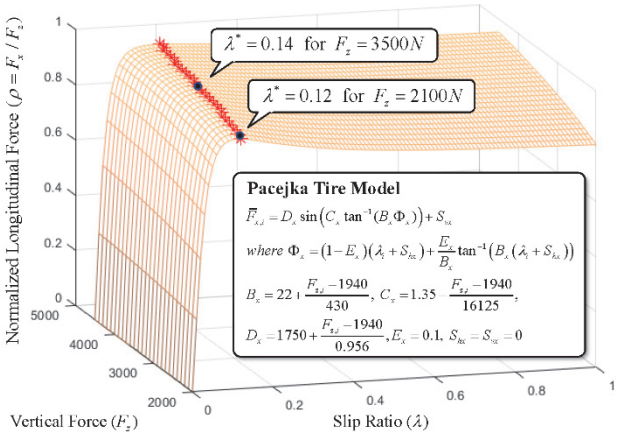

Figure 5. 3D map of the Pacejka tire model.

$$\begin{aligned} T_{bc,2} = & -J_{w,2} \cdot (1+\lambda_2) \cdot \dot{\omega}_{v,2} - r_{eff} \cdot \bar{F}_{x,2} \\ & - J_{w,2} \cdot \omega_{v,2} \cdot \dot{\lambda}_2^* + K_2 \cdot J_{w,2} \cdot \omega_{v,2} \cdot \mathrm{sgn}(s_2) \end{aligned} \tag{32}$$

$$\begin{aligned} T_{bc,3} = & -J_{w,3} \cdot (1+\lambda_3) \cdot \dot{\omega}_{v,3} + T_{e,3} - r_{eff} \cdot \bar{F}_{x,3} \\ & - J_{w,3} \cdot \omega_{v,3} \cdot \dot{\lambda}_3^* + K_3 \cdot J_{w,3} \cdot \omega_{v,3} \cdot \mathrm{sgn}(s_3) \end{aligned} \tag{33}$$

$$\begin{aligned} T_{bc,4} = & -J_{w,4} \cdot (1+\lambda_4) \cdot \dot{\omega}_{v,4} + T_{e,4} - r_{eff} \cdot \bar{F}_{x,4} \\ & - J_{w,4} \cdot \omega_{v,4} \cdot \dot{\lambda}_4^* + K_4 \cdot J_{w,4} \cdot \omega_{v,4} \cdot \mathrm{sgn}(s_4) \end{aligned} \tag{34}$$

where $\bar{F}_{x,i}$ is the nominal tire force model from (2).

5. SIMULATION ENVIRONMENTS

5.1. Scenarios

The simulations for the original SMC and SMC-based NDOB were conducted using CarSim software with an RWD vehicle, whose nominal parameters are listed in TAB. 2. Each simulation was performed in two constant-friction road braking scenarios (high/low) chosen based on the guidelines given by TAB.1 according to United Nations Regulation 13 (Pretagostini *et al*., 2020).

5.2. Key Performance Indicators

To compare the braking performance, three key performance indicator (KPI) sets were selected as follows:

Brake distance (BD) - The absolute brake distance, determined by integrating the velocity from the initial time t_i to a finite time t_f, is given by

$$BD = \int_{t_i}^{t_f} v_x dt \tag{35}$$

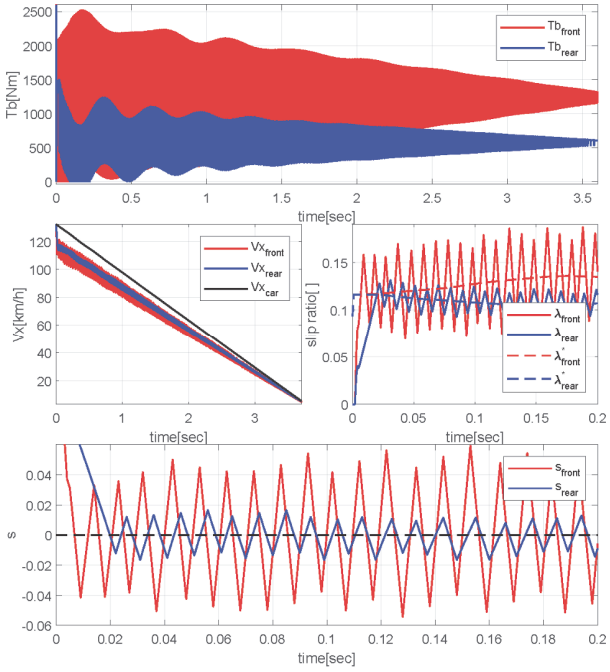

Figure 6. SMC results in the high- μ scenario.

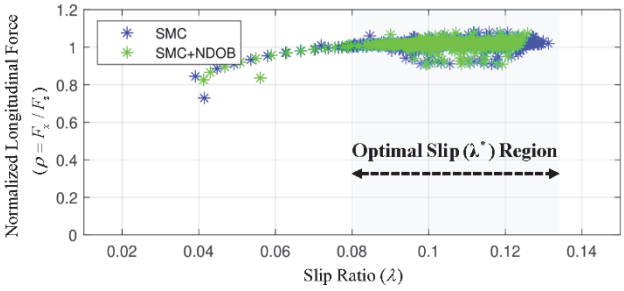

Figure 7. Normalized force via the slip ratio for high μ.

Integral torque variation – Actuator wear($IACA_{T_b}$) - The braking torque variation related to the actuator wear is given by

$$IACA_{T_b} = \int_{t_i}^{t_f} \sum_k \left| \dot{T}_{b,k} \right| \, dt \qquad k = [FL, FR, RL, RR] \tag{36}$$

Integral square error(ISE) – The usual criteria for the control performance index are given by

$$ISE = \int_{t_i}^{t_f} e^2(t) \, dt \qquad e(t) = r(t) - y(t) \tag{37}$$

The simulation results in the next subsection will be discussed based on the above KPIs.

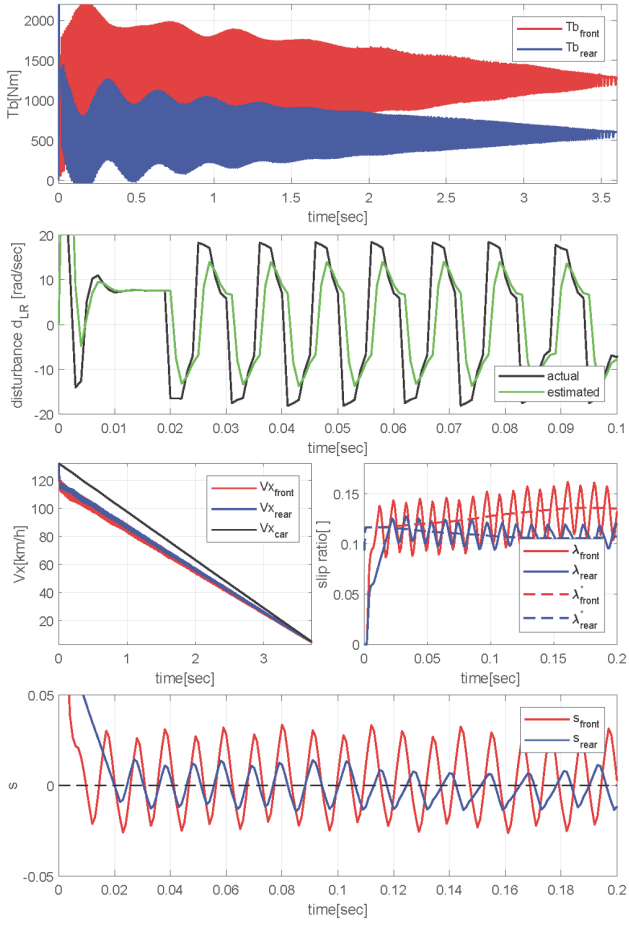

Figure 8. SMC results with NDOB in the high- μ scenario.

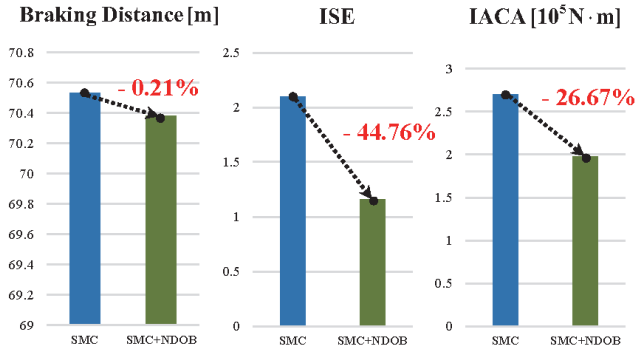

Figure 9. KPI results in the high- μ scenario.

5.3. Optimal Reference Slip (λ_i^*) for Each Tire

To obtain the maximum braking performance, the optimal reference slip λ_i^* should be derived from the tire model. The optimal reference slip can be expressed as a function of the vertical load since the tire longitudinal force F_x depends on the vertical load F_z. Figure 5 shows the 3D map of the

Pacejka tire model, which is given in eqn. (2). The optimal reference slip λ_i^* is 0.12 for F_z = 2100 N, and λ_i^* is 0.14 for F_z = 3500 N. Therefore, the optimal reference slip can be derived and the curve fitted with a polynomial function with F_z as a variable. The function curve fitted by the MATLAB curve-fitting toolbox *cftool* is given as follows:

$$\lambda^*(F_z) = (1.03e-12)F_z^3 - (5.377e-9)F_z^2 + (1.548e\text{-}5)F_z + 0.09355 \tag{38}$$

In the simulation, it was assumed that all four tires [FL, FR, RL, RR] were identical with 225/60 R18.

Additionally, F_z for each tire is known during simulation.

6. SIMULATION RESULTS

6.1. Simulation Results in the High-μ Scenario

Based on Sections 2 ~ 5, the simulation results obtained with basic SMC and SMC with an NDOB in the high-μ scenario are shown in Figures 6 and 8, respectively. The control input is the braking torque T_b of each wheel, and the ideal situation assumes that latency in generating the braking torque does not exist. Since the left and right sides of the vehicle are symmetrical, the controller gain is the same ($K_1 = K_2 = K_f$, $K_3 = K_4 = K_r$. According to the high-μ scenario described in Pretagostini *et al*. (2020), the simulation was performed with 130 km/h as the initial speed and 5 km/h as the terminal speed. The optimal reference slip λ^* for each tire is given by Equation (38).

Figure 7 shows the normalized force via the slip ratio of SMC and SMC+NDOB during the simulations. It is shown that the slip ratio of the systems stays within the boundary of the optimal slip region. Figure 6 shows the conventional SMC results with K_f =54 and K_r = 24. Based on (35) ~ (37), the KPIs were recorded as BD = 70.53 m, $IACA = 2.70 \cdot 10^5 N \cdot m$ and ISE = 2.10. These results are presented in Figrue 9 as a bar graph. As seen from the braking torque T_b in Figure 6, there exists a severe chattering problem in the control input. The chattering issue can be alleviated by choosing a lower SMC gain when compensating for the uncertainty using NDOB.

Figure 8 shows the results for SMC based on NDOB with lower gains, which are K_f = 17 and K_r = 12 . The KPIs were recorded as BD = 70.38 m, $IACA = 1.98 \cdot 10^5 N \cdot m$ and ISE = 1.16, as shown in Figure 9. Based on Equation (25), the estimated disturbances, including the rolling resistance and modelling error, asymptotically converge to the real disturbances of the system. The observer gain $\mathbf{L}$ is selected as a bandwidth of 100 Hz. As a result of choosing a lower SMC gain when applying the NDOB, BD decreased by 0.21 % and ISE decreased by 44.76 %, so it can be concluded that the control performance increased. Furthermore, as the chattering decreased, it was shown that $IACA$ decreased significantly, by 26.67 %. This means that the life of the brake pads is prolonged. For verification in more diverse situations, a simulation on a low-μ road is conducted with the same controllers in the next subsection.

6.2. Simulation Results in the Low-μ Scenario

On a low-μ road surface, the simulation results with conventional SMC and SMC with the NDOB are shown in Figures 10 and 12, respectively. Similar to the previous high-μ scenario, the control input is the braking torque T_b of each wheel, and it is assumed that latency in generating the braking torque does not exist. The simulation was conducted with 40 km/h as the initial speed and 1 km/h as the final speed. Additionally, the optimal reference slip is given by (38), and the average friction coefficient is 0.3.

Figure 10 shows the SMC results with gains $K_f = 51$ and $K_r = 35$. Figure 12 shows the results for SMC with the NDOB with gains $K_f = 16$ and $K_r = 15$, which are lower than those of the method with only SMC. In the low-μ scenario simulation, the input braking torque T_b reaches 1600 $N \cdot m$, which is smaller than that in the high-μ scenario because of the lower initial speed. Figure 11 shows the normalized force via the slip ratio, and it is proven that the slip ratio of the systems stays at the boundary of the optimal slip region.

Figure 13 shows the KPI results for the low-μ scenario. BD decreases slightly, by 0.15 %, from 6.47 m to 6.46 m. ISE decreases by 31.34 %, from 0.67 to 0.46. And $IACA$ decreases significantly, by 31.69 %, from $2.84 \cdot 10^5 N \cdot m$ to $1.94 \cdot 10^5 N \cdot m$, similar to the previous high-μ simulation.

7. CONCLUSION

In this paper, sliding mode control based on a nonlinear disturbance observer for an anti-lock braking system is proposed, and simulations of high- and low-μ scenarios are conducted. Because of the mechanical structure of the ABS module and unknown road environments, sliding mode control techniques are applied in industry to achieve robustness and reduced tuning time. However, the basic sliding mode controller has a severe chattering problem due to unknown disturbances, which leads to wear of the mechanical brake pads. To address the chattering issue, the unknown disturbances can be estimated and compensated for by a real-time estimator, which is called a nonlinear disturbance observer. Three KPIs are selected: the braking distance, integral square error for ABS performance and integral torque variation for actuator wear.

For verification in various situations, high- and low-μ

scenarios are tested on CarSim software. As a result, *BD* and *ISE* decrease slightly, which indicates enhanced control performance. In particular, *IACA* is shown to decrease. The detailed performances and parameters of the simulation results are listed in Table 3. This leads to the extension of the life of the braking pads. However, there is a limitation of the absence of experimental verification in real situations considering latency. Additionally, in real experiments, the tire force model or vertical force for each tire should be estimated. These are major issues in vehicle control.

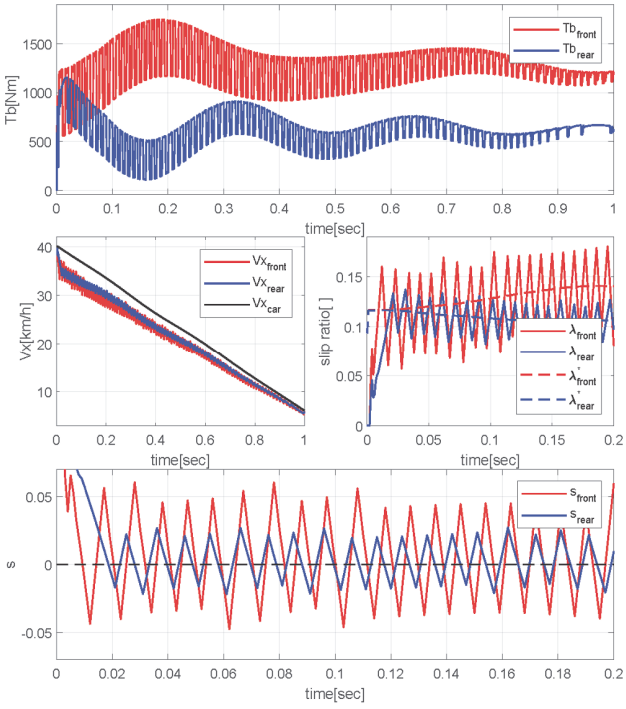

Figure 10. SMC results in the low- μ scenario.

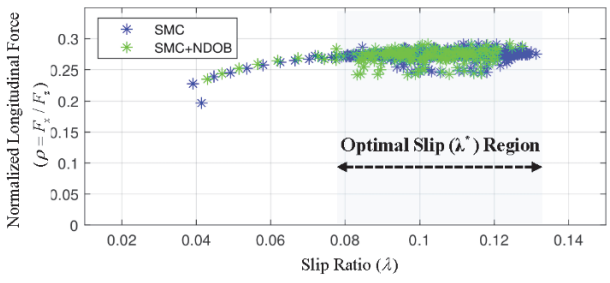

Figure 11. Normalized force via the slip ratio for low- μ .

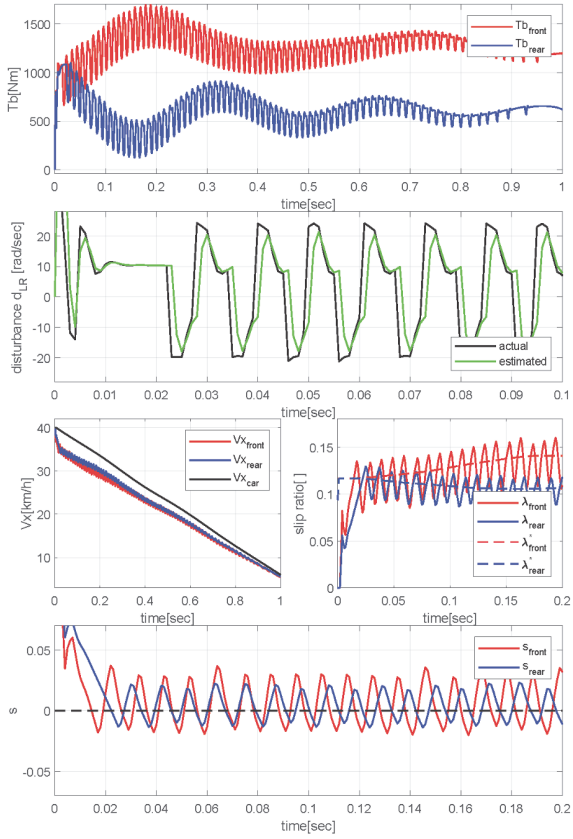

Figure 12. SMC results with the NDOB in low- μ scenario.

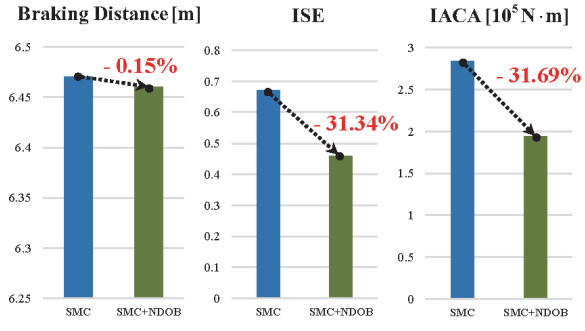

Figure 13. KPI results in the low- μ scenario.

Table 3. Summary of simulation results.

Parameters	High- μ Scenario		Low- μ Scenario	
	SMC	SMC +NDOB	SMC	SMC +NDOB
K_f	54	17	51	16
K_r	24	12	35	15
BD	70.53 m	70.38 m	6.47 m	6.46 m
ISE	2.10	1.16	0.67	0.46
IACA	2.70 · 10^5 *Nm*	1.98 · 10^5 *Nm*	2.84 · 10^5 *Nm*	1.94 · 10^5 *Nm*

ACKNOWLEDGEMENT–This research was financially supported by the Institute of Civil Military Technology Cooperation and funded by the Defense Acquisition Program Administration and Ministry of Trade, Industry and Energy of the Korean government under grant No. UM19303RD3.

REFERENCES

Aripin, M. K., Md Sam, Y., Danapalasingam, K. A., Peng, K., Hamzah, N. and Ismail, M. F. (2014). A review of active yaw control system for vehicle handling and stability enhancement. *Int. J. Vehicular Technology*, **2014**, 437515.

Bosch, R. and Peter (Tr.) Girling (1996). *Automotive Handbook.* 10th edn. Plochingen. Cambridgeshire.

Cai, J. W., Liang, C. H. U., Cheng, W. F. and Wang, Y. B. (2012). Modeling and simulation of ABS hydraulic control unit. *2nd Int. Conf. Electronic & Mechanical Engineering and Information Technology (EMEIT)*, Shenyang, China.

Chen, C. K. and Shih, M. C. (2004). PID-type fuzzy control for anti-lock brake systems with parameter adaptation. *JSME Int. J. Series C Mechanical Systems, Machine Elements and Manufacturing* **47**, **2**, 675–685.

Chen, W. H., Ballance, D. J., Gawthrop, P. J. and O'Reilly, J. (2000). A nonlinear disturbance observer for robotic manipulators. *IEEE Trans. Industrial Electronics* **47**, **4**, 932–938.

Choi, S. B. (2008). Antilock brake system with a continuous wheel slip control to maximize the braking performance and the ride quality. *IEEE Trans. Control Systems Technology* **16**, **5**, 996–1003.

Gao, Z. (2014). On the centrality of disturbance rejection in automatic control. *ISA Trans.* **53**, **4**, 850–857.

Jazar, R. N. (2017). *Vehicle Dynamics: Theory and Application.* 3rd edn. Springer. Riverdale, NY, USA.

Kachroo, P. and Tomizuka, M. (1995). Sliding mode control with chattering reduction and error convergence for a class of discrete nonlinear systems with application to vehicle control. *Proc. Int. Mechanical Engineering Cong. Expo*, San Francisco, California, USA.

Kiencke, U. and Nielsen, L. (2000). *Automotive Control Systems: For Engine, Driveline, and Vehicle*. 2nd edn. Springer. Karlsruhe, Germany.

Kim, S. W. and Lee, J. J. (1995). Design of a fuzzy controller with fuzzy sliding surface. *Fuzzy Sets and Systems* **71**, **3**, 359–367.

Kuang, M. L., Fodor, M., Hrovat, D. and Tran, M. (1999). Hydraulic brake system modeling and control for active control of vehicle dynamics. *American Control Conf. (ACC)*, Louis, MO, USA.

Layne, J. R., Passino, K. M. and Yurkovich, S. (1993). Fuzzy learning control for antiskid braking systems. *IEEE Trans. Control Systems Technology* **1**, **2**, 122–129.

Lennon, W. K. and Passino, K. M. (1999). Intelligent control for brake systems. *IEEE Trans. Control Systems Technology* **7**, **2**, 188–202.

Li, S., Yang, J., Chen, W. H. and Chen, X. (2014). *Disturbance Observer-based Control: Methods and Applications*. CRC Press. Boca Raton, New Jersey, USA.

Lin, C. M. and Hsu, C. F. (2003). Self-learning fuzzy sliding-mode control for antilock braking systems. *IEEE Trans. Control Systems Technology* **11**, **2**, 273–278.

Lojko, B. and Fuchs, P. (2002). *The Control of ASR System in a Car Based on the TMS320F243 DSP*. Ph. D. Dissertation. Dept. of Radio & Electronics, Bratislava, Slovakia.

Mauer, G. F. (1995). A fuzzy logic controller for an ABS braking system. *IEEE Trans. Fuzzy Systems* **3**, **4**, 381–388.

Pacejka, H. B. and Bakker, E. (1992). The magic formula tyre model. *Vehicle System Dynamics* **21**, **S1**, 1–18.

Pretagostini, F., Ferranti, L., Berardo, G., Ivanov, V. and Shyrokau, B. (2020). Survey on wheel slip control design strategies, evaluation and application to antilock braking systems. *IEEE Access*, **8**, 10951−10970.

Sariyildiz, E. and Ohnishi, K. (2014). A guide to design disturbance observer. *J. Dynamic Systems, Measurement, and Control* **136**, **2**, 021011.

Slotine, J. J. E. and Li, W. (1991). *Applied Nonlinear Control*. Prentice Hall. Englewood Cliffs, New Jersey, USA.

Unsal, C. and Kachroo, P. (1999). Sliding mode measurement feedback control for antilock braking systems. *IEEE Trans. Control Systems Technology* **7**, **2**, 271–281.

Vignati, M. and Sabbioni, E. (2020). Force-based braking control algorithm for vehicles with electric motors. *Vehicle System Dynamics* **58**, **9**, 1348–1366.

Wellstead, P. E. and Pettit, N. B. O. L. (1997). Analysis and redesign of an antilock brake system controller. *IEEE Proc.-Control Theory and Applications* **144**, **5**, 413–426.

Will, A. B. and Zak, C. S. H. (2000). Antilock brake system modelling and fuzzy control. *Int. J. Vehicle Design* **24**, **1**, 1–18.

Wong, J. Y. (2008). *Theory of Ground Vehicles.* 3rd edn. John Wiley & Sons. New York, NY, USA.

Yang, S., Lu, Y. and Li, S. (2013). An overview on vehicle dynamics. *Int. J. Dynamics and Control* **1**, **4**, 385–395.

Zhu, H., Zhang, G. and Shao, H. (2005). Control of the process with inverse response and dead-time based on disturbance observer. *American Control Conf. (ACC)*, Portland, Oregon, USA.